Plastic Collapse of Cylinders Under Constrained Conditions

A. Abdul-Latif
ERBEM,
Université Paris 8,
IUT de Tremblay,
93290 Tremblay-en-France,
France
e-mail: aabdul@iu2t.univ-paris8.fr

K. Nesnas
GSM/LASMIS,
Université de Technologie de Troyes,
B.P. 2060,
10010 Troyes cedex,
France

This paper deals with an experimental methodology of the large deformation of cylinders under constrained sides and end conditions. A specific arrangement of two geometrically identical cylinders compressed laterally is studied under different quasi-static strain rates. Several tests are performed using two different structural situations. In the first case, the two cylinders are made from superplastic tin-lead alloy, while in the second case, one cylinder is made from superplastic and the other from steel. Different cylindrical geometries are investigated having the same cross sectional area with different ratios of inner to outer diameter (di/do). The load-deflection curves are recorded and then the energy absorbed per unit volume is determined. The experiments show obviously the remarkable sensitivity of the utilized superplastic to the strain rate in the range of $10^{-5}/s-10^{-3}/s$. *A two-dimensional finite element simulation is also conducted describing the collapse behavior of these cylindrical geometries in both structural cases under different strain rates. A confrontation with experimental observation shows that the predictions describe fairly well the experiments.* [DOI: 10.1115/1.1543970]

I Introduction

Since the past three decades, a great number of impact engineering problems has been investigated focusing notably on the dynamic response of structures in the plastic range. Devices utilizing large plastic deformation are widely used as a mean of absorbing energy and have a substantial role to play in the improvement of aircraft crashworthiness and vehicular collisions [1] with the objective of minimizing human suffering and financial losses. A number of literature surveys representing the state of the art in this field (e.g., [2–7]) give detailed discussions of the techniques and theoretical treatments of different absorbing devices.

Large plastic behavior of mechanical elements (plates, shells, tubes, stiffeners,..) when subjected to various types of load has been the subject of several experimental and theoretical researches over the last decades. The main goal of these investigations is to better understand the modes of deformation, then the resulting failure and the energy dissipation patterns during collapses. Note that the majority of the structures are subjected predominantly to compressive loads. For any given device, the capability to absorb the energy depends, in general, on the magnitude, type and method of application of loads, strain rates, deformation or displacement patterns and material properties [4]. Moreover, each device has its own characters and features, so to understand the material response during collapse, the plastic flow (collapse mechanisms) should be well determined through experimental procedures.

Cylindrical tubes are deformable elements, which lead themselves to a wide variety of applications such as energy absorbers. They can be plastically buckled under the action of axial load; theories for the buckling in the plastic region (zone in which the plastic strain is well localized leading to plastic hinges) were suggested under static and dynamic loads ([8–12,6,13] and others). They can be also plastically flattened along their common tangent under compressive load (e.g., [14–20]), turned inside out (tube inversion) ([21–24] and others). Hence, the crushing (axially or laterally) of cylinders has received a great deal of attention in the contest of energy dissipating systems.

Recently, studies have been carried out concerning the large plastic collapse of cylinders employing a special rig without constrained sides and end conditions under different strain rates [25–26]. As a complementary study, the aim of this work is to experimentally investigate the capability of a new proposed mechanical device (Fig. 1) in absorbing the energy and to understand the large plastic collapse mechanisms of the structures under lateral compressive load in the case where the sides and the end of cylinders are constrained. The same cylinders as in [25,26] with different inside/outside diameter ratios ($R=di/do$) ranging from 0 to 0.473, are tested under different strain rates in the range of $10^{-5}/s-10^{-3}/s$. Two different structural situations are studied. In the first case, both cylinders are made from superplastic tin-lead alloy (deformable-deformable situation) referred to as (DD), while in the second case, one cylinder is superplastic and the other is steel. In this case referred to as deformable-nondeformable situation (DND), the steel cylinder deforms elastically during the test, while the superplastic cylinder deforms plastically. The numerical prediction is made through the finite element technique modeling

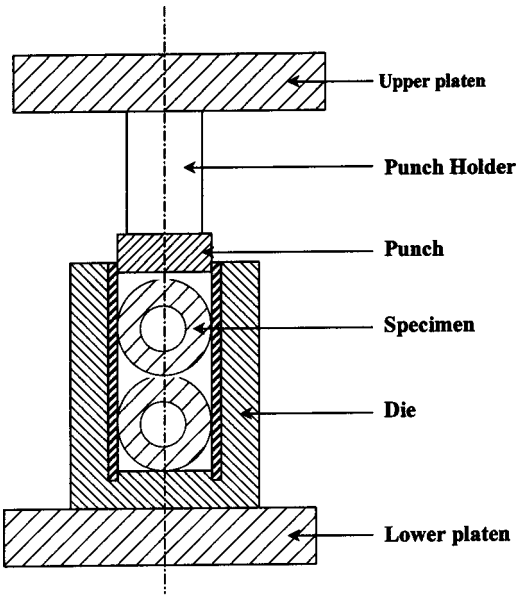

Fig. 1 Sectioned view of the assembled rig of the constrained situation tests

Contributed by the Materials Division for publication in the JOURNAL OF ENGINEERING MATERIALS AND TECHNOLOGY. Manuscript received by the Materials Division December 4, 2001; revision received July 3, 2002. Associate Editor: H. M. Zbib.

the lateral collapse of two geometrically identical cylinders. Numerical solutions are carried out in finite rate-dependent plasticity (viscoplasticity) adopting the assumptions of plane strain and the Norton-Hoff's law as material behavior. The FE technique can appropriately reproduce the observed plastic flow, compressive force and energy absorbed evolutions during the plastic deformation of cylinders at different strain rates. Such simulations are conducted with a commercial finite element code FORGE2 (Forge2 user's manual). This leads, despite the geometric assumption and the simplicity of the employed constitutive law, to describe appropriately the collapse behavior of the cylinders.

II Experimental Procedure and Results

Cylindrical specimens of different (R) values are made from superplastic tin-lead alloy (61.9 percent–38.1 percent by weight). They are produced by forward extrusion with about 80 percent reduction having almost the same cross-sectional area. A length of 20 mm is always discarded after extrusion giving specimen lengths of 60 mm. For further details on the production technique of the cylindrical specimens, the reader is to refer to the reference (Abdul-Latif, 2000). The final dimensions of the employed cylinders are listed in Table 1.

The experimental tests are conducted using a special rig (Fig. 1). The whole specimens are loaded between the platens of an Instron Universal Testing Machine at three constant cross head speeds, 0.2, 5, and 20 mm/min, giving almost according to Abdul-Latif [25] the representative strain rates of 7×10^{-5}/s, 1.8×10^{-3}/s and 7×10^{-3}/s, respectively. In order to ensure the experimental results accuracy, each test is repeated twice under the same experimental conditions (applied speed and temperature). All tests are systematically conducted at the room temperature. If the difference between the two responses exceeds three percent, then another test has to be performed. For each case of R, three tests are conducted under increasing loading at different strain rates given above. Figures 2 and 3 show some selected load-deflection behaviors in the case of DD and DND, respectively. The variation of the energy absorbed per unit volume with R ratio is experimentally pointed out in Figs. 4 and 7 for a given axial displacement for DD and DND, respectively. In order to study the flow mechanism in the case of DD and DND, the collapsed cylinders were sectioned, polished, projected on a profile projector at a magnification of ten and then traced. Figure 8 shows traces of

Table 1 Dimensions of tested cylinders

No.	(do), mm	(di), mm	di/do (R)	length 10, mm	volume, mm^3
1	24.4	0.0	0.0	60	28055,7
2	24.9	5.08	0.204	60	28001,2
3	25.5	7.2	0.283	60	28199,4
4	26.1	9.1	0.348	60	28198,9
5	27.7	13.1	0.473	60	28070,8

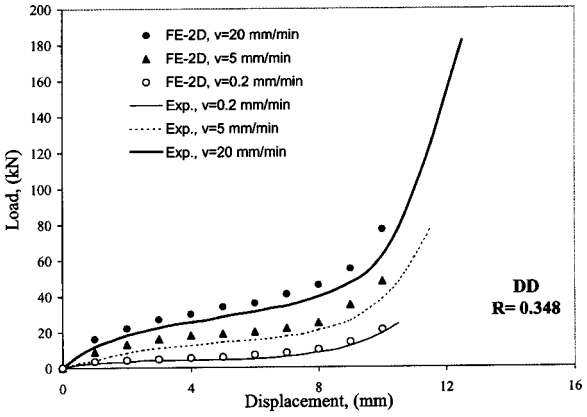

Fig. 2 Load-deflection characteristics at different strain rates in the deformable-deformable (DD) situation for the specimens of $R=0.348$

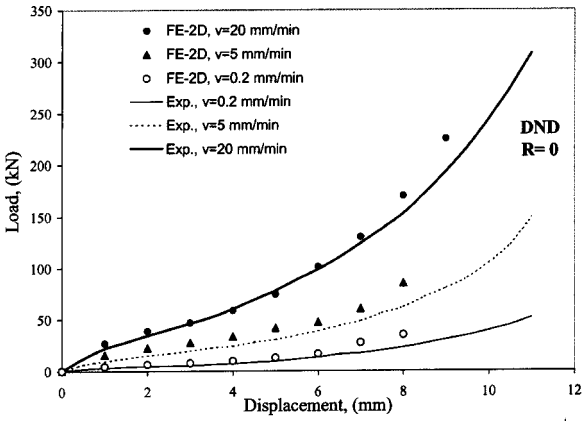

Fig. 3 Load-deflection characteristics at different strain rates in the deformable-nondeformable (DND) situation for the specimens of $R=0$

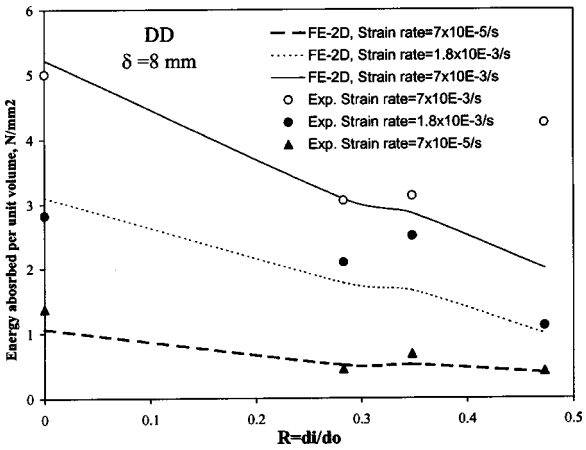

Fig. 4 Variation of energy absorbed per unit volume versus R for the deformable-deformable (DD) situation under the three strain rates for $\delta=8$ mm

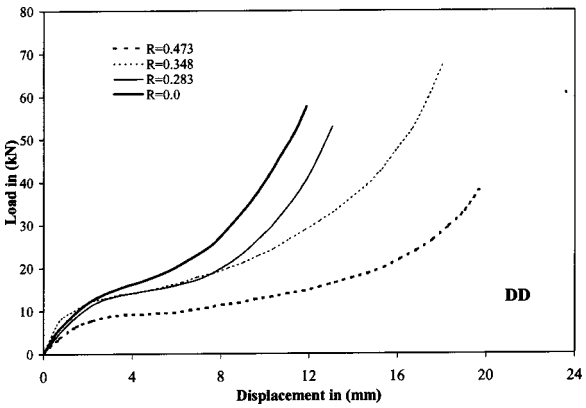

Fig. 5 Experimental comparison between the mechanical behaviors of the four used cylinders in the deformable-deformable case under representative strain rate of 7×10^{-3}/s

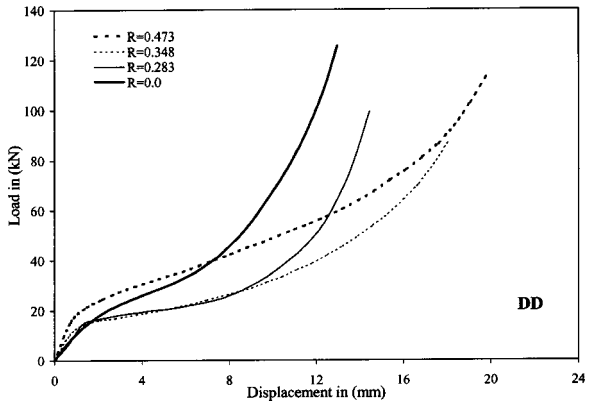

Fig. 6 Experimental comparison between the mechanical behaviors of the four used cylinders in the deformable-deformable case under representative strain rate of 1.8 $\times 10^{-3}$/s

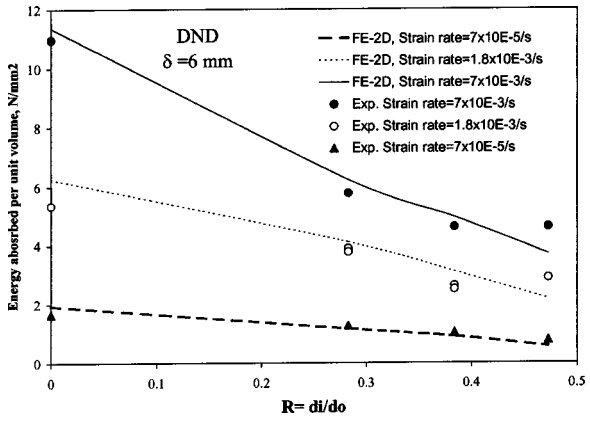

Fig. 7 Variation of energy absorbed per unit volume versus *R* for the deformable-nondeformable (DND) situation under the three strain rates for δ=6 mm

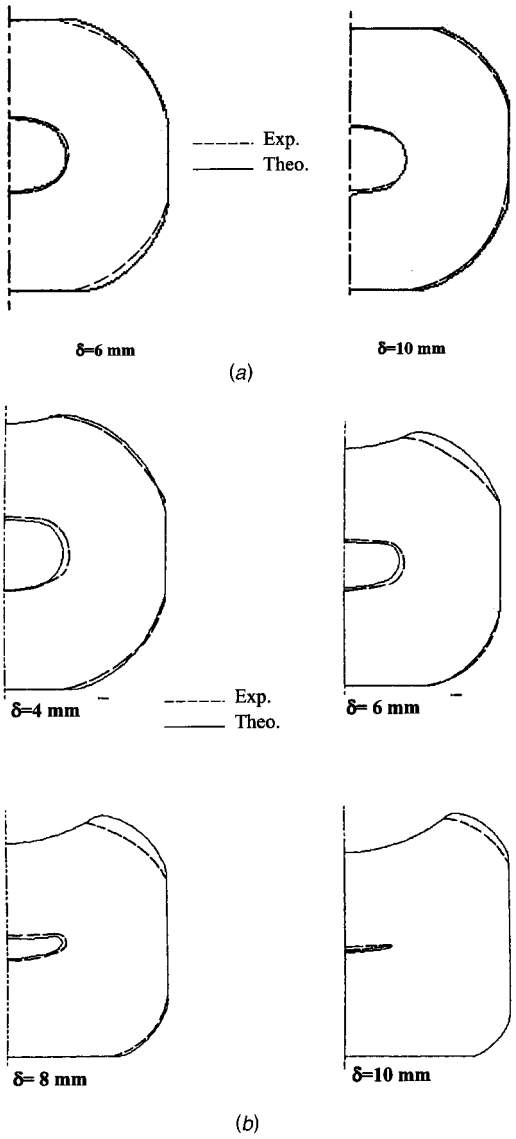

Fig. 8 Profiles of projected cross sections of hollow cylinders at $R=0.348$ after deformation in (*a*) DD and (*b*) DND situations (numerical and experimental comparison)

cross sections of a cylinder having $R=0.348$ at different axial displacements under the strain rate of 1.8×10^{-3}/s for both structural situations (DD and DND).

III Basic Formulation

For many years, a number of different approaches for finite element simulation of large deformation of mechanical part have been presented. These approaches differ in several fundamental aspects. Such differences can be with respect to kinematic description, constitutive description and solution methodology. In this paper, the two-dimensional finite element code (FORGE2) is based on the flow approach with a rigid viscoplastic model, where the stress is expressed in terms of strain rates. The approach is based on an updated Lagrangian description, where the geometry is fixed in each time step while equilibrium is iteratively solved. The geometry is then updated based on the calculated nodal velocities. In the following, an all-encompassing presentation of the constitutive law and finite element formulation are given demonstrating the basic equations of the numerical prediction, especially, the dissipated energy expression.

III.1 Constitutive Model. Many constitutive equations have been proposed for superplastic materials [27–28]. The level of sophistication of the model employed must be weighed with accuracy and efficiency considerations as well as the qualitative and quantitative knowledge of the material. A fairly accurate representation of the superplastic material behavior is required to make analysis results meaningful.

The most important effect in any superplastic constitutive model is the rate dependence. Superplastic flow is a creep phenomenon, which for uniaxial loading is approximately described by the equation:

$$\sigma = 2K(\sqrt{3}\dot{\varepsilon})^m \varepsilon^n G^p \tag{1}$$

where σ, ε, and $\dot{\varepsilon}$ are the uniaxial stress, strain and strain rate, respectively. G is a parameter defining the grain size. K, m, n, and p are the material parameters. Thermal effects, grain size evolution and distribution effects should also be included as other level of sophistication. In this paper, n (strain hardening exponent) is taken equal to zero. This is a good approximation since n is small in reality. For simplification, the equivalent flow stress may be regarded in three-dimensional case as a function of the strain rate only as follows:

$$\boldsymbol{\sigma}^d = 2K((\sqrt{3}d)^{m-1}\mathbf{D} \tag{2}$$

where $\boldsymbol{\sigma}^d$ is the deviator of the Cauchy stress tensor $\boldsymbol{\sigma}$, $\mathbf{D}$ is the strain rate tensor and $\bar{d}=\sqrt{2/3(D:D)}$.

This expression is known as the Norton-Hoff's law. The main influencing factor is the exponent m, which measures the strain rate sensitivity of the material.

III.2 Finite Element Formulation. The rate problem can be represented by the deformation of a given domain (Ω) between one fixed tool Γ_0 and another movable tool Γ_{tool}, which is assumed to be rigid and moving with a velocity V_{tool}. The material (Ω) is assumed to be homogeneous, isotropic, incompressible and its behavior is given by (Eq. 2), whereas the boundary traction is zero on the free boundary Γ_{free}, the contact zones between the tools (Γ_0 and Γ_{tool}) and the work piece is modeled with contact conditions. On the tools, the nonpenetration condition is given by:

$$(\mathbf{v}-\mathbf{v}_{\text{die}})\cdot\mathbf{n}=\mathbf{v}_s\cdot\mathbf{n}=0 \tag{3}$$

If the reversible friction displacement is neglected, a viscoplastic friction behavior can be used. It is described by a nonlinear relation between the shear stress $\boldsymbol{\tau}$ and the tangential velocity difference $\mathbf{v}_s$ at the tool part interfaces Γ_0 and Γ_{tool}:

$$\boldsymbol{\tau}=-\alpha_f K|\mathbf{v}_s|^{q-1}\mathbf{v}_s \tag{4}$$

where, α_f is the friction coefficient and q, which is often equal to m, represents the sensitivity index to the sliding velocity.

The virtual power principle gives the integral form for any virtual velocity field $\mathbf{v}^*$:

$$\int_\Omega \boldsymbol{\sigma}:\mathbf{D}^* dV+\int_\Omega \rho\mathbf{f}\mathbf{v}^* dV-\int_{\Gamma_0\cup\Gamma_{\text{tool}}}\boldsymbol{\tau}\mathbf{v}^* dS=0 \tag{5}$$

where, $\mathbf{f}$ is the volumic force and $\mathbf{D}^*$ is the virtual strain rate tensor. In order to satisfy the incompressibility condition, the penalty formulation is often used:

$$\int_\Omega \sigma:\mathbf{D}^* dV+\int_\Omega \rho\mathbf{f}\mathbf{v}^* dV-\int_{\Gamma_0\cup\Gamma_{\text{tool}}}\boldsymbol{\tau}\mathbf{v}^* dS + \int_\Omega \rho_p \,\text{div}(\mathbf{v})\text{div}(\mathbf{v}^*)dV=0 \tag{6}$$

with ρ is a sufficiently large penalty constant and

$$\text{div}(\mathbf{v})=\mathbf{I}:\mathbf{D} \tag{7}$$

is the rate of volume change per unit volume. $\mathbf{I}$ is the identity tensor.

Using the classical displacement (velocity) based on finite element method with isoparametric elements, the following linear interpolation function has been used:

$$\mathbf{v}=\sum_{\mathbf{n}}\mathbf{N}_{\mathbf{n}}(\xi)\mathbf{V}_{\mathbf{n}},\quad \mathbf{v}^*=\sum_{\mathbf{n}}\mathbf{N}_{\mathbf{n}}(\xi)\mathbf{V}_n^*,\quad \mathbf{D}=\sum_{\mathbf{n}}\mathbf{B}_{\mathbf{n}}(\xi)\mathbf{V}_{\mathbf{n}} \tag{8}$$

the penalty formulation (Eq. 6) is immediately discritised into:

$$\int_{\Omega_t} 2K(\sqrt{3}\bar{d})^{m-1}\mathbf{D}:\mathbf{B}_{\mathbf{n}}dV+\int_{\Omega_t}\rho\mathbf{f}\,\mathbf{N}_{\mathbf{n}}dV + \int_{(\Gamma_0\cup\Gamma_{\text{tool}})_t}\alpha_f K|\mathbf{v}_s|^{q-1}\mathbf{v}_s\mathbf{N}_n dS+\int_{\Omega_t}\rho_p\,\text{div}(\mathbf{v})\text{tr}(\mathbf{B}_{\mathbf{n}})dV=0 \tag{9}$$

where ξ are the local coordinates, $\mathbf{N}_{\mathbf{n}}$ the shape functions, $\mathbf{B}_{\mathbf{n}}$ the shape function gradients, and $\mathbf{V}_{\mathbf{n}}$ the nodal velocity vectors.

These equations are solved by a Newton-Raphson iterative procedure using sub-incrementation when necessary. An explicit integration scheme is used to update the configuration. The nodal coordinates are then updated by writing:

$$\mathbf{X}_{t+\Delta t}=\mathbf{X}_t+\mathbf{V}(t)\Delta t \tag{10}$$

Moreover, the total dissipated energy dissipation of the deformation process at the time t is determined using the following expression in the case of the Norton-Hoff's friction law (Eq. 4).

$$\mathbf{W}=\int_{t_0}^{t}\left(\int_\Omega K(\sqrt{3}\bar{d})^{m+1}dV+\int_{(\Gamma_0\cup\Gamma_{\text{tool}})_t}\alpha_f K|\mathbf{v}_s|^{q+1}dS\right)dt \tag{11}$$

III.3 Remeshing. With an updated Lagrangian formulation, the nodes of the mesh follow the kinematic evolution of the material points. This method leads to a highly distorted mesh due to the large deformation of the material. When the final topology is very different from the initial one, the same mesh topology is generally not convenient for the whole process. For these reasons, remeshing (available in FORGE2) becomes mandatory and takes place frequently in some examples (it can be more than 300 meshes). Therefore, a new mesh is automatically generated as soon as one of the following criteria are reached: (i) distortion of a finite element or a segment of the boundary; (ii) bad description of the die-part interface; (iii) large curvature of the segments of the free boundary; and finally, (iv) detection of a fold.

IV Results and Discussion

In the case of two deformable cylinders (DD), different experimental tests are conducted investigating the effect of the specimen geometry and the strain rate on the mechanical collapse of the structure.

As a typical example, Fig. 2 shows the load-deflection curves for $R=0.348$. In this case, a rapid evolution of the lateral compressive force is recorded for small axial deflections followed by an almost plateau region and then by a final rapid force evolution. This figure displays an increasing of the compressive force with the strain rate increasing for a given deflection. Reflected undoubtedly by the material rate sensitivity, the divergence of the load-deflection curves is distinctly observed with increasing deflection. Moreover, at any particular load, the plastic strain increases as the R ratio is increased. Similarly, at any particular deflection, the required load is also increased as the strain rate increases.

As in [25,26], the structural geometry of the cylinder (R) plays also a considerable role in dissipating the energy for the current developed device. Fig. 4 displays the evolution of the energy absorbed per unit volume versus R for a selected axial deflection of 8 mm. In general, the energy absorbed is mainly consumed at the beginning by a flattening process in the contact zone between the two cylinders, then, with more increasing δ, the flattening takes place at the constraining walls of the rig and in the radial flow which causes the closure of the bore. Due to a change in the flow mechanism for $R=0.473$ at the strain rate of 1.8×10^{-3}/s and 7×10^{-3}/s, the energy absorbed increases rapidly at the strain rate of 7×10^{-3}/s, decreases under the strain rate of 1.8×10^{-3}/s and becomes almost stable for the smallest strain rate. It is obvious now that the flow mechanism of the superplastic changes notably for structures having $R\geqslant0.348$ as in [25]. In order to better understand this observation, a comparison between the mechanical behaviors of the four different cylinders is conducted at the strain rate of 7×10^{-3}/s (Fig. 5). For the axial deflections more than 10 mm, the flow mechanism changes just after the plateau region where the collapse behavior is completely diverged especially for $R=0$ and 0.283 with respect to $R=0.348$ and 0.473. In addition, the cylinders of $R=0.283$ and 0.348 behave almost similarly up to an axial deflection around 9 mm (Fig. 5). The similarity of the collapse behavior between 0.283 and 0.348 remains valid up to $\delta=8$ mm at the strain rate of 1.8×10^{-3}/s as demonstrated in Fig. 6, then, a distinct divergence between these structures is appropriately shown. Therefore, it is recognized that the collapse behavior of the cylinder is principally governed by the geometrical factor (R) and the applied strain rate.

The flow mechanism of the deformable cylinder of $R=0.348$, for example, is studied under the strain rate of 1.8×10^{-3}/s at two selected axial deflections of 6 and 10 mm (Fig. 8(*a*)). Under these selected deflections, the bore closure does not completely occur, but the plastic strain, especially for $\delta=10$ mm, is generally localized in certain zones around the bore.

For the deformable–nondeformable (DND) case, the same strain rates and R ratio are used as in the DD case. The experimental load-deflection curves are presented in Fig. 3 for $R=0$ (as an example). Each structure is tested under these strain rates. Fig. 3 shows the same finding obtained in the DD case, i.e., the greater the strain rate, the lower the ratio R, the greater the required force is needed for a given deflection. The curves diverge with increasing deflection due to the change in the strain rate. This reflects the material sensitivity to the strain rate especially in the range of 10^{-4}/s–10^{-3}/s [29].

The variation of the energy absorbed per unit volume with respect to R for a given axial deflection (6 mm) is shown in Fig. 7. Note that an important part of the energy is consumed by the indentation of the steel cylinder in the superplastic one, i.e., the horizontal flattening is eliminated and replaced by indentation. Another part of energy is absorbed during the flattening of deformable cylinder at constraining walls. For $R=0.348$, the rate of charge of the energy absorbed for any given axial deflection is decreased especially for the strain rate of 1.8×10^{-3}/s. Whereas, for $R=0.473$, the energy absorbed slightly increases under the strain rate of 1.8×10^{-3}/s compared with those results obtained in the case of $R=0.348$. This is related to the change of the plastic collapse mechanism for $R\geqslant0.348$.

Concerning the flow mechanism, four successive deformed states (for axial deflections: 4, 6, 8, and 10 mm) are displayed in Fig. 8(*b*) revealing the real progressive mechanism of the bore closure related directly with the amount of the imposed axial deflection at the strain rate of 1.8×10^{-3}/s. Note that a relatively complete bore closure takes place for $\delta=10$ mm.

The focus of the finite element simulation is to check the possibility to predict the experimental plastic collapse of the tubes system of constrained sides and end described previously. The idea is to adopt the two-dimensional plane strain and employing the Norton-Hoff's law to reproduce the main phenomena encountered in such process. Although, the problem is three-dimensional, it appears that the plane strain assumption gives generally an acceptable prediction of the flow mechanism and energy absorbing capacity. The simulated cases are selected in such a manner that the combination of the principal influenced parameters are appropriately taken into account like geometrical and compressive strain rate as well as the structural situations (DD and DND) specified in the previous section. These structures exhibit generally several important features such as: (i) nonhomogeneous deformations; (ii) variable regions of contact between deformed cylinders and rig; (iii) the variation of the strain rate at material points; and (iv) rapid rise of total rig force when an important part between the cylinders and the rig is in contact.

For the finite element analysis, based on the geometrical symmetry, only one half part of the specimen is descritized with six-node elements. Fig. 9 displays the undeformed meshes in both cases of DD and DND situations (with a hollow cylinder). The die is modeled as a rigid surface. The number of elements is varying according to the treated case (233 to 376 elements). The density values of meshes are 5 to 26 meshes.

In actual compression test, it is difficult to determine the exact frictional condition at the interface between the die and cylinders. Therefore, some simulations are performed for one case of cylinder geometry with the DD situation under the frictional condition specified by the following friction coefficients:

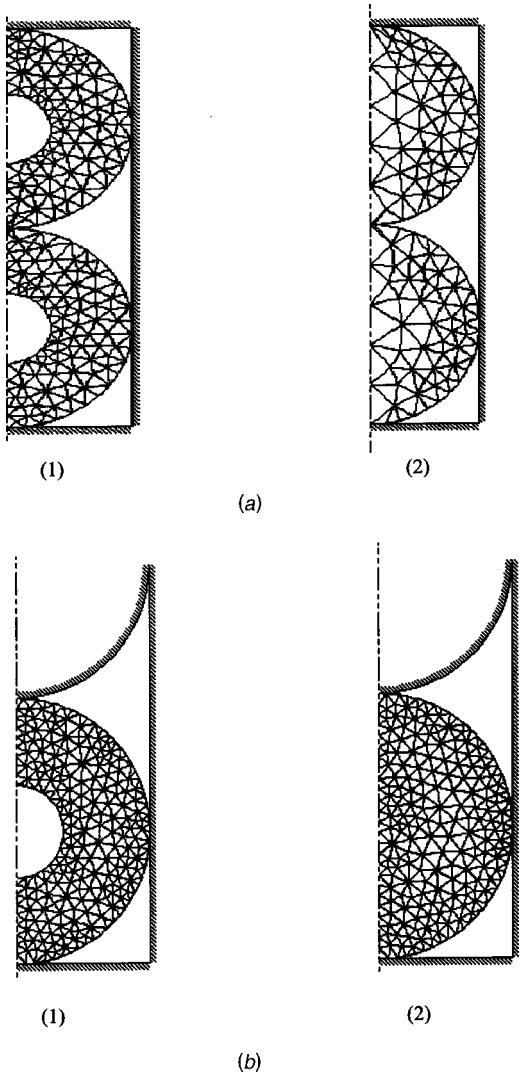

Fig. 9 Finite element mesh for (*a*) DD situation for (1) $R=0.348$, (2) $R=0$ and (*b*) DND situation for (1) $R=0.348$, (2) $R=0$

0.0, 0.05, and 0.3. By comparing the results on the load deflection curves, it has been noticed that the load agrees reasonably well with lower deflection ($\delta<9$ mm), but differences are recorded at higher deflections. Since the most comparison with experimental results are performed under the deflection of $\delta=10$ mm, the rest of simulations are thus performed under frictionless condition. Moreover, the model parameters (material consistency (K) and the strain rate sensitivity (m)) have been already calibrated by Abdul-Latif [25] giving respectively $K=180$ MPa and $m=0.395$.

Many aspects are going to be investigated in this finite element simulation under quasi-static loading conditions. It can be noted from examination of Figs. 2 and 3, for $R=0$ and 0.348 for both DD and DND situations, that the load-deflection curves indicate that the predictions describe fairly well the experimental results notably the rate dependence. Note that jumps in load occur in the predicted result whenever new nodes come into contact with the die.

Figures 4 and 7 reveal that, within the experimental limitations, the energy absorbed per unit volume for each system increases as the strain rate is increased for all values of R. In the DD situation, the finite element method can not reproduce the sudden change in energy absorption capability for $R=0.473$. This is, as we think,

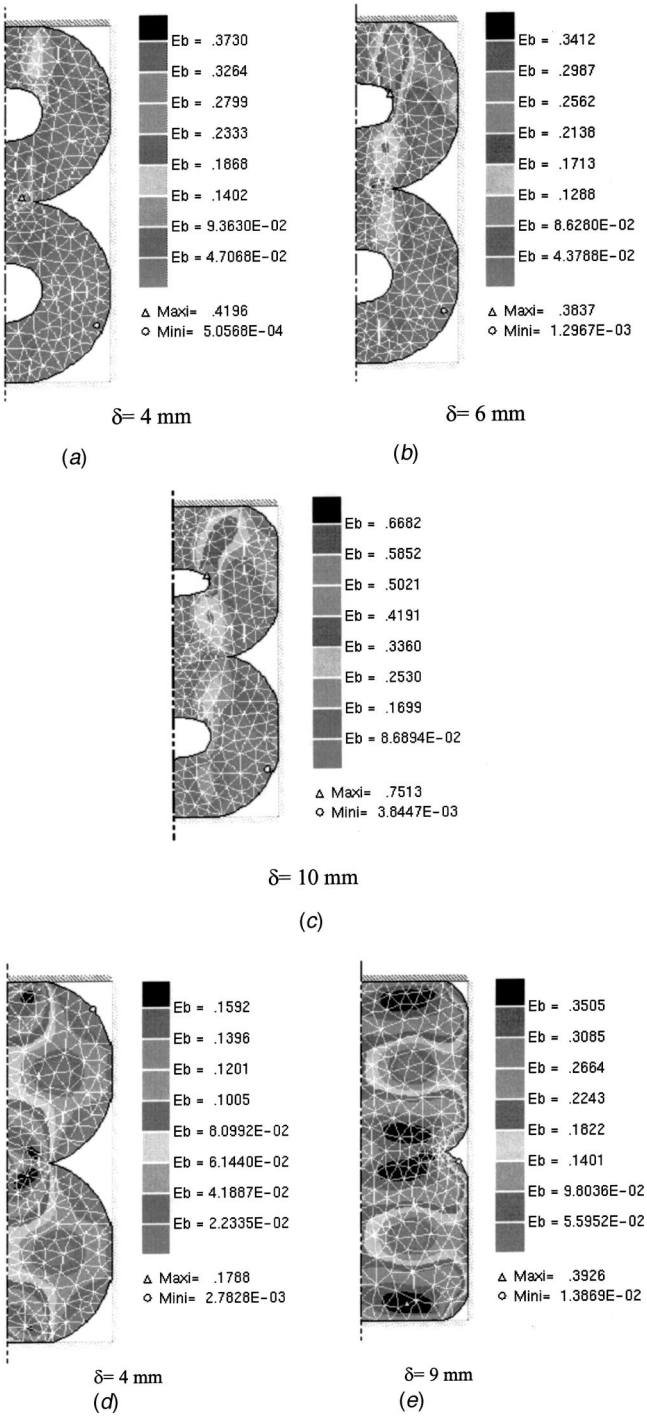

Fig. 10 Plastic strain distribution at compressive speed of 5 mm/min for $R=0.348$ (*a*) $\delta=4$, (*b*) $\delta=4$, (*c*) $\delta=10$ mm, $R=0$, (*d*) $\delta=4$, and (*e*) $\delta=9$ mm in the case of DD situation

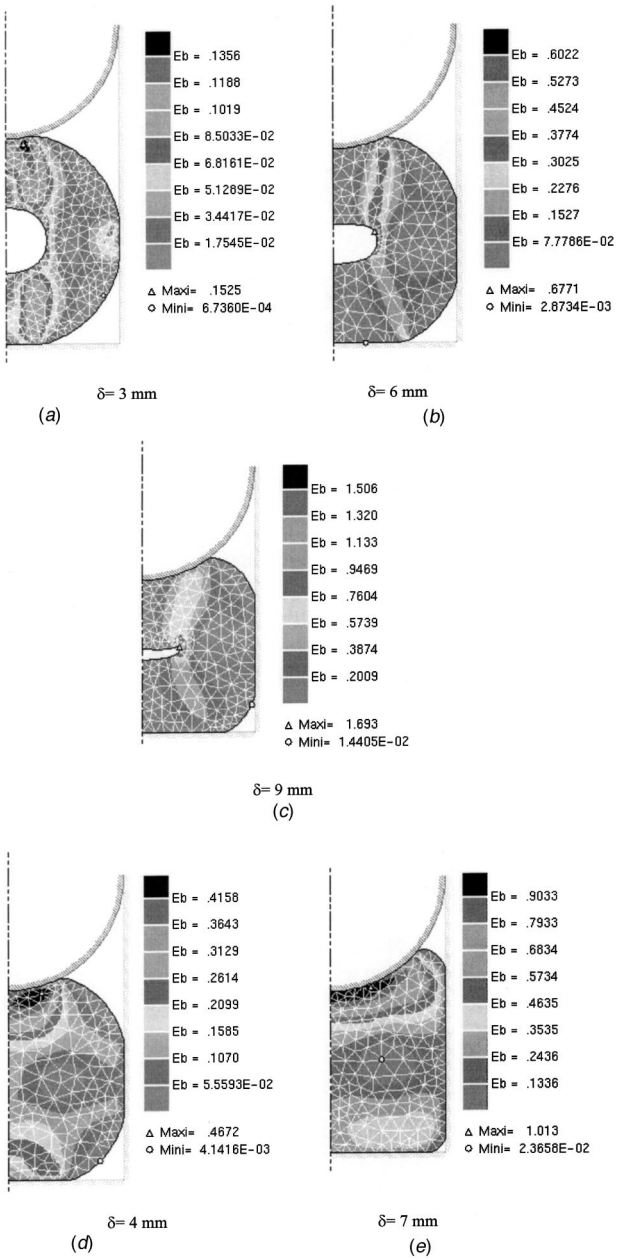

Fig. 11 Plastic strain distribution at compressive speed of 5 mm/min for $R=0.348$ (*a*) $\delta=3$, (*b*) $\delta=6$, (*c*) $\delta=9$ mm, $R=0$, (*d*) $\delta=4$, and (*e*) $\delta=7$ mm in the case of DND situation

due to the simplicity of the Norton-Hoff's law, which neglects the hardening phenomenon and the adopted two-dimensional plane strain. For the DND situation, it is obvious that the numerical results describe fairly well the variation of the energy absorbed with R ratio at different strain rates notably for $R<0.473$ (Fig. 7).

Figure 8 shows both the numerical and experimental results of deformed cylinders profiles during different successive deformed states for the DD and DND situations, in the case of $R=0.348$. It displays that the simulation reproduces almost correctly the mode of deformation. In fact, the deformed cylinder has acquired a shape (external and bore boundaries), which agrees quite well with the experimental one. Particularly, for the DND case, where the bore is not completely closed at $\delta=6$ mm, but at 10 mm the bore closure is almost terminated.

In the case of $R=0.348$, the distribution of the accumulated plastic strain is presented, as an example, in Figs. 10 and 11, for the DD and the DND situations respectively at different deflections. In spite of the difference between the DD and the DND situations in their plastic flow mechanisms, the cylinders (for both cases), however, suffer from a plastic strain in their commune contact region less important than that in certain zones around the bore (Figs. 10(*b*), and (*c*) and Figs. 11(*b*) and (*c*). The flow mechanism that develops towards the bore direction undergoes plastic strain localization (plastic hinges) in the lateral extremities of the deformed bore. These plastic hinges are often observed in another case of tube crushing [26]. Hence, they can be considered as zones in which the damage will be initiated and then evolved up to the final fracture.

V Conclusions

Motivated by its sensitivity to the quasi-static strain rate (10^{-5}/s to 10^{-3}/s), the superplastic tin-lead alloy is used to represent the behavior of metallic materials in the intermediate and high strain rates.

A new metallic energy absorbing device is proposed in which the large plastic collapse of cylinders with constrained sides and end conditions is studied under lateral compressive load from experimental and numerical points of view. The experimental investigations show that the strain rate and the geometry of cylinders (R ratio) have a remarkable role on the plastic collapse mechanism and the absorbed energy whatever the structural situation, i.e., DD or DND. The capability of the system to absorb the energy is generally increased by increasing the strain rate and decreasing the ratio R for the same volume and cross-sectional area. Under the same load and strain rate, the amount of deflection in the specimen decreases almost with the decrease in the R ratio. Moreover, for both structural situations, the flow mechanism around the cylinder bore of the deformable cylinder is studied at a given strain rate showing successively the bore closure mechanism under different selected deflections.

This experimental study is supported by a numerical analysis based on the simple Norton-Hoff's constitutive equation as a model describing the plastic behavior of superplastic alloy and its sensitivity to the strain rate. Therefore, the numerical analysis of the collapse behavior of the cylinders show acceptable predictions of several experimental aspects, namely, the flow mechanism and absorbed energy.

However, the actual modeling can not reproduce the eventual change in the plastic collapse mechanism for $R \geqslant 0.348$ especially in the deformable-deformable case. Therefore, it will be a judicious choice when more experimental investigations will be carried out with a more sophisticated viscoplastic constitutive law and three-dimensional finite element simulation to improve the predicted results.

References

[1] Hermann, G., and Perrone, G., 1972, *Dynamic Response of Structures*, Pergamon Press.

[2] Ezra, A. A., and Fay, R. J. 1970, *An Assessment of Energy Absorbing Devices for Prospective Use in Aircraft Impact Situation*, Dynamic Response of Structures, G. Hermann and N. Perrone eds., Pergamon Press.

[3] Rawlings, B., 1974, ''Response of Structures to Dynamic Loads,'' Proc. Conf. On Mechanical Properties of Materials at High Rates of Strain, Institute of Physics Conference, pp. 279–298.

[4] Johnson, W., and Reid, S. R., 1978, ''Metallic Energy Dissipating Systems,'' Appl. Mech. Rev., **31**, pp. 277–288.

[5] Johnson, W., and Reid, S. R., 1986, ''Metallic Energy Dissipating Systems,'' Rev. 31, pp. 277–288; Appl. Mech. Update 1986, pp. 315–319.

[6] Jones, N., 1989, *Structural Impact*, Cambridge Press, Cambridge, UK.

[7] Alghamdi, A. A. A., 2001, ''Collapsible Impact Energy Absorbers: An Overview,'' Thin-Walled Struct., **39**, pp. 189–213.

[8] Alexander, J. M., 1960, ''An Approximate Analysis of the Collapse of Thin Cylindrical Shells Under Axial Loading,'' Q. J. Mech. Appl. Math., **13**, pp. 11–16.

[9] Pugsley, A. G., and Macaulay, M., 1960, ''The Large Scale Crumpling of Thin Cylindrical Columns,'' Q. J. Mech. Appl. Math., **13**, pp. 1–9.

[10] Batterman, S. C., 1968, ''Free-Edge Plastic Buckling of Axially Compressed Cylindrical Shell,'' ASME J. Appl. Mech., **35**, p. 73.

[11] Abramowicz, W., and Jones, N., 1986, ''Dynamic Progressive Buckling of Circular and Square Tubes,'' Int. J. Impact Eng., **4**, pp. 243–270.

[12] Reid, S. R., Reddy, T. Y., and Gray, M. D., 1986, ''Static and Dynamic Axial Crushing of Foam-Filled Sheet Metal Tubes,'' Int. J. Mech. Sci., **28**, pp. 295–322.

[13] Reddy, T. Y., and Al-Hassani, S. T. S., 1993, ''Axial Crushing of Wood-Filled Square Metal Tubes,'' Int. J. Mech. Sci., **35**, pp. 231–246.

[14] DeRutz, J. A., and Hodge, J. R., 1963, ''Crushing of a Tube between Rigid Plates,'' ASME J. Appl. Mech., **30**, pp. 391–395.

[15] Rewood, R. G., 1964, ''Discussion of ref. (DeRutz & Hodge (1963)),'' ASME J. Appl. Mech., **31**, pp. 357–358.

[16] Johnson, W., Reid, S. R., and Reddy, T. Y., 1977, ''The Compression of Crossed Layers of Thin Tubes,'' Int. J. Mech. Sci., **19**, pp. 423–437.

[17] Reddy, T. Y., and Reid, S. R., 1979, ''Lateral Compression of Tubes and Tube-Systems with Side Constraints,'' Int. J. Mech. Sci., **21**, pp. 187–199.

[18] Reid, S. R., Drew, S. L. K., and Carney, J. F., 1983, ''Energy Absorbing Capacities of Braced Metal Tubes,'' Int. J. Mech. Sci., **25**, pp. 649–667.

[19] Shim, V. P.-W., and Stronge, W. J., 1986, ''Lateral Crushing in Tightly Packed Arrays of Thin-Walled Metal Tubes,'' Int. J. Mech. Sci., **28**, pp. 709–722.

[20] Wu, L., and Carney, III, J. F., 1998, ''Experimental Analysis of Collapse Behaviors of Braced Elliptical Tubes under Lateral Compression,'' Int. J. Mech. Sci., **40**, pp. 761–777.

[21] Al-Hassani, S. T. S., Johnson, W., and Lowe, W. T., 1972, ''Characteristics of Inversion Tubes under Axial Loading,'' J. Mech. Eng. Sci., **14**, pp. 370–381.

[22] Kinkead, A. N., 1983, ''Analysis for Inversion Load and Energy Absorption of a Circular Tube,'' J. Strain Anal., **18**, pp. 177–188.

[23] Reddy, T. Y., 1989, ''Tube Inversion- an Experiment in Plasticity,'' Int. J. Mech. Engng. Educ., **17**, pp. 277–292.

[24] Reid, S. R., 1993, ''Plastic Deformation Mechanisms in Axially Compressed Metal Tubes Used as Impact Energy Absorbers,'' Int. J. Mech. Sci., **35**, pp. 1035–1052.

[25] Abdul-Latif, A., 2000, ''On the Lateral Collapse of an Identical Pair of Cylinders,'' Int. J. Solids Struct., **37**, pp. 1955–1973.

[26] Nesnas, K., and Abdul-Latif, A., 2001, ''Lateral Plastic Collapse of Cylinders: Experiments and Modeling,'' Computer Modeling in Engineering and Sciences, **2**, pp. 373–388.

[27] Bellet, M., 1988, ''Modélisation Numérique du Formage Superplastique des Tôles,'' Ph.D. thesis, Ecole Nationale Supérieure des Mines de Paris.

[28] Mingwang, F., and Luo, Z. J., 1996, ''The Simulation of the Viscoplastic Forming Process by the Finite Element Method,'' J. Mater. Process. Technol., **55**, pp. 442–447.

[29] Al-Naib, T. Y. M., and Duncan, J. L., 1970, ''Superplastic Metal Forming,'' Int. J. Mech. Sci., **12**, pp. 463–477.